Elegant Way of Strengthening Polymer–Polymer Interface Using Nanoclay

Ganesh C. Basak,[†] K. Dinesh Kumar,[†] Abhijit Bandyopadhyay,[‡] and Anil K. Bhowmick*[,†,§]

Rubber Technology Centre, Indian Institute of Technology, Kharagpur 721302, India, and Department of Polymer Science and Technology, University of Calcutta, Calcutta 700 009, India

ABSTRACT A unique mechanism responsible for enhancing the autohesive tack strength of ethylene propylene diene rubber (EPDM) was elucidated by studying the interfacial strength of an unvulcanized EPDM elastomer joint in the presence of nanoclay. The tack strength significantly increased with nanoclay concentration up to 4 parts per 100 grams of rubber (phr), beyond which it dropped. For example, the tack strength of 4 phr of the nanoclay-loaded sample was nearly 137% higher than that of neat EPDM rubber. The influence of nanoclay in the bond formation and the bond separation steps of the tack test was understood by analyzing various tack governing factors such as green strength, creep compliance, entanglement molecular weight, relaxation time, the self-diffusion coefficient, and the monomer friction coefficient (ζ_0). Furthermore, the ability of EPDM rubber to undergo strain-induced crystallization (SIC) during straining (at the time of bond separation in the peel test experiment) in the presence of nanoclay was also investigated. When the clay concentration was 4 phr, there was a slight reduction in the extent of molecular diffusion at the tack junction due to the nanoclay reinforcement; however, the diffusion was sufficient enough to establish entanglements across the interface. Furthermore, the less diffused chains of the nanocomposite samples showed greater bond breaking resistance than the unfilled sample due to the higher ζ_0 value owing to the nanoclay reinforcement. It was also observed that the presence of nanoclay reduced the amount of crystallinity in the unstrained state and hence favored diffusion of elastomer chains across the interface. In addition, the presence of nanoclay significantly increased the ability of the EPDM elastomer to crystallize due to the alignment of nanoclay during straining, thus providing greater bond breaking resistance to the diffused elastomer chains. At higher clay loading (>4 phr), the elastomer chains could not establish entanglements across the interface due to extremely slow diffusion and aggregated platelets on the rubber surface, and therefore the tack strength decreased.

KEYWORDS: EPDM • autohesive tack • reinforcement • nanoclay • rubber

INTRODUCTION

The diffusion of one polymer into another plays an important role in many industrial processes, ranging from melt blending of miscible polymers to friction welding and heat sealing in plastics (1). The development of adhesion across polymer–polymer interfaces depends on the diffusion of polymer molecules across the interface so that they become entangled on both sides (1). The case where the polymers on either side of the interface are chemically identical is termed autohesion. For instance, it has been shown in the literature that if two halves of a fractured specimen of polymethylmethacrylate (PMMA) are placed in contact, the fracture toughness of the joint increases as $t^{0.5}$ (where t is the contact time) (1). On the other side, when two unvulcanized rubber surfaces of similar chemical composition are brought into intimate contact for a short period of time under light pressure, interdiffusion of elastomer chains takes place across the interface, and the diffused chains show some resistance to separation. This phenomenon is termed autohesive tack (1–5). It was reported earlier that the following conditions must be met by a rubber compound for exhibiting high tack (3): (a) the two rubber surfaces must come into intimate molecular contact; (b) diffusion of polymer chains across the interface must take place; (c) the bonds thus formed must be capable of resisting high stress before rupture. This tack property is of great importance in the tire industry and certain other rubber industries, where it enables different parts of multicomponent rubber articles to be fabricated more easily and to remain in the assembled condition prior to the final curing process. Among the class of elastomers, natural rubber (NR) possesses the highest degree of autohesive tack, and other elastomers, in particular ethylene propylene termonomer (EPDM) and styrene butadiene rubber (SBR), have very little tack (3).

Generally, external modifiers such as oil, tackifiers, and fillers are found to have a significant effect on the tack strength of elastomers (3). Plasticizers like oil facilitate molecular diffusion across the interface by reducing the entanglement density of the rubber chains, but diluted, interdiffused rubber chains are more easily separated than the unfilled rubber, and hence the tack strength reduces (3). Tackifying resins are added at low concentrations in rubber compounds to enhance tack in synthetic elastomers and to prevent the decay of tack in the naturally tacky elastomer like natural rubber during aging (3). Similar to the action of

* Corresponding author. Tel.: +91 3222 283180/91 612 2277380. Fax: +91 3222 220312/91 612 2277384. E-mail: anilkb@rtc.iitkgp.ernet.in, director@iitp.ac.in.

Received for review July 18, 2010 and accepted September 28, 2010

[†] Indian Institute of Technology.

[‡] University of Calcutta.

[§] Present Address: Indian Institute of Technology, Patna 800013, India.

DOI: 10.1021/am100865n

oil, tackifying resins also reduce the entanglement density of the base elastomer. However, the interdiffused chains diluted with tackifiers resist separation significantly more than those diluted with oil, and hence the tack strength increases (6−10). However, clear understanding of the effect of changes of surface and bulk viscoelastic properties of an elastomer by the addition of tackifiers on the autohesive tack strength has been fraught with lot of interrelated factors. Very recently, research workers from our own group proposed a mechanism to exploit the interplay between the changes in surface energy and bulk viscoelastic properties of the base elastomer by the addition of tackifiers to achieve a desired tack value (10). In literature, it has also been shown that the addition of reinforcing fillers like carbon black can increase the tack strength of elastomers (3, 11−15). For example, the addition of 40 phr of carbon black to NR resulted in a significant increase in the tack strength of NR (11). On the other hand, the addition of carbon black to SBR resulted in a significant reduction in the tack strength (3). Therefore, it was concluded that the effect of carbon black addition on tack depends more on the elastomers' ability to achieve bond formation, rather than its specific chemical nature (3).

The literature contains many references stating that EPDM rubber possess insufficient tack because of the branching of the EPDM chains combined with their high entanglement density, which can drastically reduce the mobility of the elastomer chains across the interface (3, 16, 17). It is well known that EPDM rubbers are capable of crystallizing under strain like NR (16). However, the tack strength values of EPDM rubber are very low when compared to NR (3). In partially crystalline EPDM rubber, crystallites are already present in the unstrained state, and therefore the chain mobility required for tack bond formation is greatly reduced (3). Finally, the question still remains whether the interdiffusion process in EPDM compounds can be slightly accelerated by some means so that the SIC phenomenon during straining can be effectively utilized to achieve a very high tack value. van Gunst et al. (16) have been successful in increasing the autohesive tack of the EPDM elastomer by adding a phenol formaldehyde resin (PFR) tackifier, by irradiation of the EPDM compound surface with visible light, preferring EPDM compounds having lower green strength and higher elongation, and finally by introducing an appropriate third monomer. Bhowmick et al. (7) have also shown that the addition of a PFR tackifier and coumarone-indene resin (CIR) tackifiers significantly increases the tack strength of EPDM rubber.

Over the past decade, polymer nanocomposites based on nanoclays have received substantial recognition due to their enhanced mechanical and physical properties compared to the conventional composites (18, 19). These nanoclays offer a wide array of property improvements at very low filler loadings owing to the dispersion of only a few nanometers-thick clay platelets of a high aspect ratio (18, 19). Currently, smectite type nanoclays are largely used in the polymer field as the reinforcing filler. In this group, montmorillonite (MMT) nanoclay has been employed in numerous polymer nanocomposite systems because it is environmentally friendly, readily available in large quantities, and its intercalation chemistry has been well studied in comparison with other nanoclays (18−20).

Our research interest lies in discovering the unique properties and structures of polymer nanocomposites containing nanofillers such as nanoclays, nanotubes, and metal nanoparticles (20−34). In line with this, we have reported recently improvement of the autohesive tack strength of brominated isobutylene-*co*-*p*-methylstyrene (BIMS) rubber with the addition of MMT and sepiolite nanoclays (35, 36). The detection of this interesting behavior of nanoclays in BIMS rubber has prompted us to initiate a detailed investigation into the tackification mechanism of nanoclay in other general purpose elastomers also. Since EPDM rubbers are known to exhibit anomalous and very poor tack when compared to other general purpose elastomers and important elastomers for the conveyor and belt industry, we report in this current work the effect of MMT nanoclay on the autohesive tack strength of EPDM rubber. Additionally, the influence of MMT nanoclay concentration on the EPDM elastomer's bond formation (self-diffusion) and bond breaking ability (strength of the interface) has been analyzed by studying various distinct tack governing parameters like crystallinity, green strength, creep compliance, entanglement molecular weight (M_e), relaxation time (τ), the self-diffusion coefficient (D), and the monomer friction coefficient (ζ_0).

Table 1. Composition of Mixes Prepared

sample number	designation	EPDM rubber (gm)	nanoclay (phr)[a]
1	EP	100	0
2	EPNA2	100	2
3	EPNA4	100	4
4	EPNA8	100	8

[a] phr = parts per 100 grams of rubber.

2. MATERIALS AND METHODS

2.1. Materials. Ethylene propylene diene rubber (EPDM with E/P 58:42 wt%/wt%) containing ethylidene norbornene as a termonomer (4.8 wt %) was procured from Uniroyal Chemicals, Middlebury, Connecticut, and unmodified sodium montmorillonite (MMT) nanoclay (grade: Cloisite Na^+) was generously supplied by Southern Clay Products, Gonzales, Texas.

2.2. Preparation of Filled Samples. Mixes were prepared in an open two-roll mill (Schwabenthan, Berlin) at room temperature. About 100 g of the EPDM rubber was dropped vertically on the bank of the roll of the mill. This was repeated until the material tended to band on the front roll. At this juncture, the nanoclay was added to the EPDM rubber, and then the mixing was continued for an additional 3 min. The normal operating speed of the front roll and back roll was kept constant at 33.6 rpm. The composition of the mixes prepared is reported in Table 1.

2.3. Preparation of Test Samples. For the determination of tack strength, rubber sheets (100-mm-wide × 150-mm-long × 2.5-mm-thick) were prepared by pressing them at 150 °C for 5 min between smooth Mylar sheets at 5 MPa pressure in

an electrically-heated press (David Bridge, Castleton, England). One side of the rubber sheet was backed by a fabric about 1-mm-thick. The samples were then left for 20 ± 2 h before testing for conditioning the samples. For the determination of maximum tensile stress, rubber sheets (100-mm-wide × 150-mm-long × 2.5-mm-thick) were prepared by pressing them at 150°C for 5 min between sheets of smooth aluminum foil at 5 MPa pressure in an electrically-heated press. For studies on morphology and dynamic mechanical properties, rubber sheets (3-cm-wide × 6-cm-long × 1.5-mm-thick) were prepared by pressing them at 150 °C for 5 min between sheets of smooth aluminum foil at 5 MPa pressure in the same electrically-heated press.

2.4. Morphology of Rubber Nanocomposites. 2.4.1. ***Wide Angle X-Ray Diffraction (WAXD) Studies.*** For the characterization of the rubber nanocomposites, XRD studies were performed using a PHILIPS X-PERT PRO diffractometer (The Netherlands) in the range 2−40° and a Cu target ($\lambda = 0.154$ nm). Then, d-spacing of the clay particles was calculated using Bragg's law. The samples were placed vertically in front of the X-ray source. The detector was moving at an angle of 2θ, while the sample was moving at an angle of θ.

2.4.2. ***Atomic Force Microscope (AFM) Imaging.*** The morphology of nanocomposite samples was analyzed by AFM. AFM studies were carried out in an open atmosphere under ambient conditions (25 °C, 60% RH) using multimode AFM from Veeco Digital Instruments, Santa Barbara, California. Topographic phase images were recorded in tapping mode atomic force microscopy (TMAFM) with a set point ratio of 0.9, using a long tapping mode etched silicon probe (LTESP) tip having a spring constant in the range of 48 N/m. For each sample, a minimum of three images were analyzed. The cantilever was oscillated at a resonance frequency (ω_0) of ∼280 kHz.

2.4.3. ***Transmission Electron Microscopy (TEM).*** The samples for TEM analysis were prepared by ultra-cryomicrotomy using Leica Ultracut UCT. Freshly sharpened glass knives with a cutting edge of 45° were used to get cryosections of 50 nm thickness. Since these samples were elastomeric in nature, the sample temperature during ultra-cryomicrotomy was kept constant at −100°C (which was well below the glass transition temperature, T_g, of the EPDM rubber), at which the samples existed in a hard glassy state, thus facilitating ultra-cryomicrotomy. The cryosections were collected and directly supported on a copper grid of 300-mesh size. The microscopy was performed later using a JEOL-2100 electron microscope (Japan), having LaB_6 filament, operating at an accelerating voltage of 200 kV.

2.5. Calculation of Surface Energy. The surface energies of neat EPDM and clay-loaded EPDM samples were calculated through contact angle (θ) measurements in a contact angle meter (Kernco, Model G-II from Kernco Instruments, EI Paso, Texas) using the Owens and Wendt equation (37−39): Bidistilled water and formamide were selected as the probe liquids. The surface parameters of these liquids were taken from the literature for calculating the contact angle (θ) (37−39). Each contact angle quoted is the mean of at least five measurements with a maximum error in θ of ±1°. All investigations were carried out in vapor saturated air at 23 ± 2 °C in a closed sample box. The equilibrium was reached in 1 min, and no variation in θ was obtained thereafter. The advancing contact angle value of the probe liquid at 5 min was recorded and reported in all cases.

2.6. Measurement of Tack Strength. The autohesive tack strength was measured by a 180° peel test. Previously, many researchers used the 180° peel test geometry for the estimation of autohesive tack strength (6−8, 10, 40). Strips (25.4-mm-wide × 75-mm-long × 2.5-mm-thick) were cut from the previously prepared sheet. A Mylar sheet was peeled just prior to testing. Tack testing was performed by placing two samples together with a Mylar insert at one end (contact area 25.4 mm × 55 mm). A load of 2 kg was applied in each case (∼14.0 kN/m^2) by means of a specially designed handpress, with a provision for applying variable loads. After sufficient contact time, the average force required to separate the two strips was measured in a computerized Zwick/Roell Z010 (Zwick/Roell, Ulm, Germany) Universal Testing Machine at 25 °C. The data were analyzed using the testXpert II software of the Zwick/Roell Universal Testing Machine. The tack strength G_a (N/m) was calculated using eq 1 (7, 8, 10)

$$G_a = 2F/w \tag{1}$$

where F is the average force (N) required for peeling and w is the width (m) of the sample. For each system, four samples were tested, and the results were averaged. In order to optimize the contact time in the tack test, the neat EPDM rubber samples were peeled at 250 mm/min at various contact times (15, 30, 60, and 120 s). The tack strength of neat EPDM marginally increased when the contact time was raised from 15 to 30 s. However, beyond 30 s of contact time, the tack strength values almost reached a plateau. Similarly, the variation of tack strength vs contact time for the clay-loaded sample (EPNA4) was also studied. Interestingly, the tack strength of EPNA4 did not increase significantly beyond 15 s of contact time. Therefore, the peel rate and contact time were kept as 250 mm/min and 15 s, respectively, for all of the samples.

2.7. Measurement of Maximum Tensile Stress from Stress−Strain Curves. Green strength was estimated by measuring the maximum tensile stress from the stress−strain curves (8, 10). Maximum tensile stress measurement was done according to the ASTM D412-98T method. Dumbbell-shaped specimens were punched from the prepared sheets, and maximum tensile stress was measured in a computerized Zwick/Roell Z010 Universal Testing Machine at 25 °C at a separation rate of 50 mm/min. The data were analyzed by testXpert II software of the Zwick/Roell Universal Testing Machine. The maximum tensile stress was taken as the maximum stress in the stress−strain, $\sigma-\varepsilon$, curve. Four samples were tested for each system, and the average of the results was reported.

2.8. Determination of Viscoelastic Properties through Dynamic Mechanical Analyzer (DMA). 2.8.1. ***Creep Compliance Measurement.*** The contact flow was measured by creep compliance measurements. The creep compliance tests were carried out in a dynamic mechanical analyzer (DMA Q 800 from TA Instruments, New Castle, Delaware) in tension mode geometry. In creep experiments, a constant stress, σ_0, of 0.025 MPa was imposed on the sample, and the resulting strain, ε, was measured as a function of time (t) at 25 °C. The sample dimensions were 6.25-mm-wide × 30-mm-long × 1.5-mm-thick. From the stress and strain, the compliance $D(t)$ of the sample can be calculated using eq 2 (41)

$$D(t) = \frac{\varepsilon(t)}{\sigma_0} \tag{2}$$

2.8.2. ***Temperature Sweep Test.*** A temperature sweep test was carried out in a dynamic mechanical analyzer (DMA Q 800 from TA Instruments) in tension mode geometry in the temperature range of −80 to +150 °C at a constant frequency of 1 Hz and at a constant strain of 0.1%. The sample dimensions were 6.25-mm-wide × 30-mm-long × 1.5-mm-thick.

2.8.3. ***Frequency Sweep Test.*** The frequency sweep tests were carried out in a dynamic mechanical analyzer (DMA Q 800 from TA Instruments) in tension mode geometry. Measurements were made at 15 frequencies in the 0.01−25 Hz range

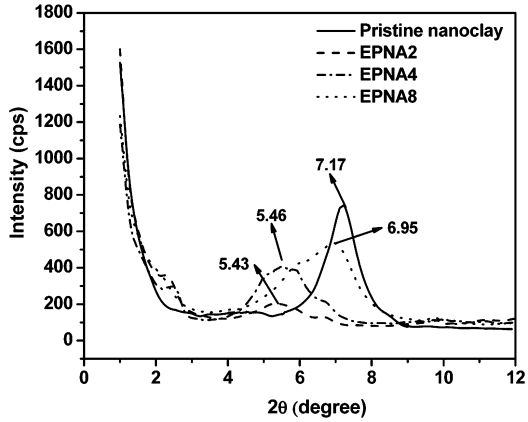

FIGURE 1. XRD patterns of pristine nanoclay and EPDM-clay nanocomposites.

at 0.1 % strain at different temperatures between −50 °C and +125 °C. All of the results were reduced to 25 °C and shifted from master curves by applying the time−temperature superposition principle, and the results were presented as storage modulus, E', and loss modulus, E'', against frequency. The sample dimensions were 6.25-mm-wide × 30-mm-long × 1.5-mm-thick.

2.9. Calculation of Radius of Gyration. The radius of gyration of neat EPDM rubber has been calculated using eq 3 (42)

$$[\eta] = \Phi\left(\frac{\langle r^2\rangle^{3/2}}{M}\right) \tag{3}$$

where $[\eta]$ is the intrinsic viscosity, $\langle r^2\rangle^{1/2}$ is the radius of gyration, and Φ is known as the Flory constant, and its value is 2.5×10^{23} mol^{-1} when $[\eta]$ is expressed in cm^3/g. M is the molar mass of the polymer (1.8×10^5 g mol^{-1}). $[\eta]$ was determined by using standard viscometric experiments (42).

3. RESULTS AND DISCUSSION

3.1. Morphology of Nanocomposites. ***3.1.1. Wide Angle X-ray Diffraction (WAXD) Studies.*** XRD diffractograms of the pristine nanoclay and the nanocomposites are shown in Figure 1. The peak for pristine nanoclay appears at 7.2° (2θ). In the case of sample EPNA2, there is a very small broad hump at 5.43°. On the other hand, the samples—EPNA4 and EPNA8—apparently show relatively larger peaks at 5.46° and 6.95°, respectively. Moreover, the height of the peak gradually increases with the concentration of the nanoclay. The measured d_{001} basal spacings of pristine nanoclay, EPNA2, EPNA4, and EPNA8 are 1.23, 1.63, 1.62, and 1.27 nm, respectively. The XRD studies suggest that in the case of samples EPNA2 and EPNA4, the EPDM rubber has intercalated into the gallery gap of the nanoclay and has expanded it, but it is unable to exfoliate the layered structure.

Previous work on nanoclay has reported that there exists difficulty in intercalating non-polar polymers into clay galleries. There are few papers in the literature which discuss the importance of modified nanoclay towards achieving an exfoliated morphology in the EPDM matrix (43). We have recently demonstrated that mixing techniques can change the morphology and dispersion of nanoclay in rubber (44). In this work, the unmodified nanoclay has been chosen because of its easy availability, and the conventionally used two-roll mill mixing technique has been found to disperse the nanoclay in the EPDM rubber up to a certain clay concentration. However, the absence of favorable interaction results in an intercalated morphology (not an exfoliated one).

On the other hand, in the case of sample EPNA8, there is evidence for the existence of agglomerated morphology. It seems that as the nanoclay loading increases, the clay particles tend to agglomerate. Agglomeration possibly starts to take place at 4 phr, which becomes prominent at 8 phr loading. Furthermore, it is well known that the surface of unmodified MMT nanoclay bears a high density of hydroxyl groups (−OH) (20). For this reason, at higher clay concentrations, there can be strong interactions among the nanoclay particles when compared to the interactions between the nanoclay and the EPDM rubber.

3.1.2. Atomic Force Microscopy. AFM phase images of samples EPNA4 and EPNA8 are shown in Figure 2. The phase image of EPNA4 (Figure 2a) shows that the clay particles are uniformly distributed in the EPDM matrix. The average width of the particles is ∼50 ± 5 nm, as observed

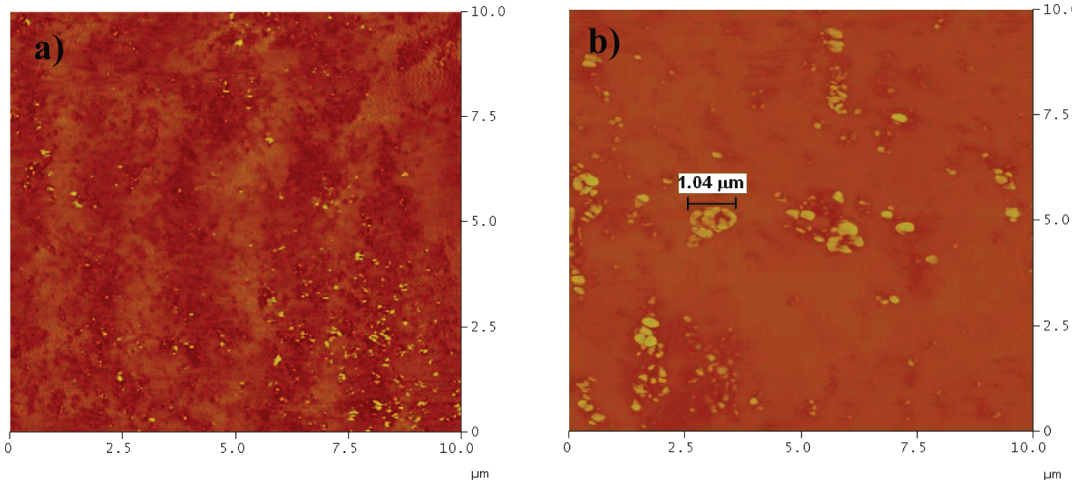

FIGURE 2. AFM phase images of (a) EPNA4 and (b) EPNA8.

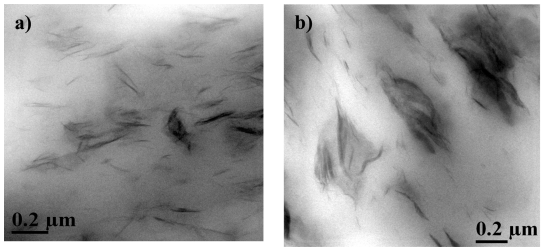

FIGURE 3. TEM micrographs of (a) EPNA4 and (b) EPNA8.

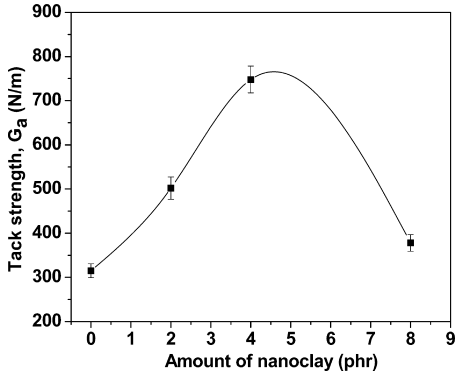

FIGURE 4. Effect of loading of nanoclay on the tack strength of EPDM rubber.

from AFM. Hence, the clay particles are mostly intercalated in the matrix along with some agglomeration. This result is in agreement with the XRD result. On the other hand, the AFM phase image of EPNA8 (Figure 2b) reveals the presence of fully agglomerated morphology. The average width of the particles is ~1.02 μm. This result is also in accord with the XRD results.

3.1.3. Transmission Electron Microscopy. TEM micrographs of samples EPNA4 and EPNA8 are shown in Figure 3. The dark lines in the micrographs are the intersectional view of the dispersed clay layers, whereas the off-white phases are the EPDM rubber matrix. The TEM micrograph of sample EPNA4 (Figure 3a) shows a homogeneous dispersion of silicate layers in the EPDM matrix along with the presence of some stacked clay particles. This clearly confirms the existence of mostly intercalated and some agglomerated clay particles at 4 phr clay loading. On the other hand, the TEM micrograph of sample EPNA8 (Figure 3b) clearly depicts the presence of agglomerated clay particles. These results are in line with the XRD and AFM results, as discussed in the previous sections.

3.2. Effect of Nanoclay Concentration on the Tack Strength of EPDM Rubber. The influence of nanoclay concentration on the tack strength of EPDM rubber is shown in Figure 4. The tack strength of EPDM rubber increases with nanoclay loading up to 4 phr, beyond which it decreases. The tack strength of the sample containing 4 phr of nanoclay is approximately 137 % higher than the tack strength of unfilled EPDM rubber. From the plot of peel force against distance curves (not shown here), it has been observed that there is an initial peak followed by a nearly constant peel force with small and random fluctuations. The peel force, F, has been taken to be the average value,

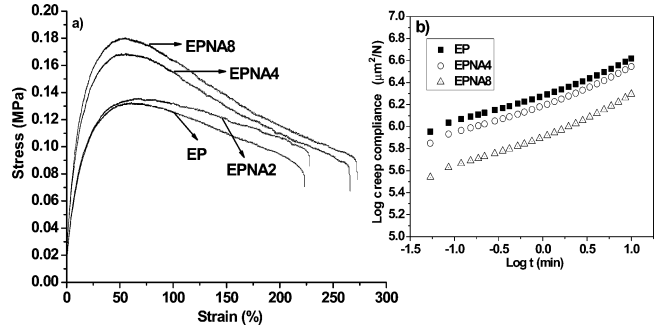

FIGURE 5. (a) Tensile stress vs strain plots of EP, EPNA2, EPNA4, and EPNA8. (Inset, b) Creep compliance of EP, EPNA4, and EPNA8.

excluding the initial peak following the procedure reported earlier (7, 8, 10, 45).

In the literature, it has been shown that the addition of 40 phr of carbon black to NR causes a substantial increase in the tack strength (3). The increase in tack strength by the addition of carbon black has been attributed to an increase in cohesive strength due to filler reinforcement, which will provide greater bond breaking resistance to the interdiffused rubber chains (3).

Interestingly, it has also been reported that the addition of carbon black to SBR and EPDM lowers the tack strength as compared to that of gum elastomers. It has already been established that a typical SBR cannot readily achieve bond formation due to the unfavorable intrinsic characters of the elastomer such as molecular weight and viscosity (3). The addition of filler further restricts the chain mobility, reducing the interfacial interactions leading to lower tack (3). The same argument can be extended for the reduction of the tack strength of EPDM rubber by the incorporation of carbon black. However, here, the addition of only 4 phr of nanoclay significantly increases the tack strength of EPDM rubber. This is a very interesting and unique observation. the addition of any reinforcing fillers will generally increase the green strength of elastomers due to the reinforcing action of the fillers. Here, there is a concomitant increase in the green strength (Figure 5a) and a reduction in the creep compliance (Figure 5b) of EPDM rubber due to the reinforcing action of the nanoclay in the EPDM matrix.

The increase in the green strength of EPDM rubber can reduce the contact flow and extent of diffusing rubber molecules across the tack interface. In spite of this, there is an increase in the tack of EPDM rubber by the addition of nanoclay. If the reduction in contact flow dominates over the enhancement in green strength, there will be a reduction in the tack strength. Therefore, in the case of the EPDM–nanoclay mixture (containing up to 4 phr of nanoclay), it can be derived that the increase in green strength dominates over the decrease in contact flow. The drop in contact flow is sufficiently low, so it is still sufficient to provide enough contact and diffusion across the interface. On the other hand, when the clay loading is greater than 4 phr, it can be envisaged that the decrease in creep compliance (contact flow) must have dominated over the increase in green strength, which can actually result in a reduction in tack

strength. Also, at 8 phr of clay concentration, there is an aggregation of nanoclay particles in the surface (see Figure 2b) as well as in the bulk (see Figure 3b). Therefore, more platelets cover the surface, and consequently polymer/polymer contact and chain diffusion will be prevented. In addition, the aggregated clay particles in the bulk will act as a topological constraint for the EPDM rubber molecules to diffuse. Therefore, at 8 phr of clay loading, the aggregated clay particles can reduce the tack strength by concomitantly preventing the polymer−polymer contact at the interface and also by reducing the mobility of the elastomer chains in the bulk.

At this juncture, it can be postulated that the increase in the tack strength of EPDM rubber by the addition of nanoclay can only be attributed to the role of nanoclay in increasing the bond breaking resistance of the diffused rubber chains. The diffused rubber chains in the clay loaded samples should show greater resistance to separation when compared to the unfilled sample due to an increase in the cohesive strength, a change in the monomer friction coefficient of the EPDM rubber by the nanoclay reinforcement, and the SIC phenomenon of EPDM rubber during straining (discussed later).

Next, we consider the other main features in the tensile stress−strain curves (Figure 5a), such as the maximum stress, σ_{max}; the strain at break, ε_b; and the work done per unit volume, W_b (area under the stress−strain, $\sigma-\varepsilon$ curve). It is instructive to determine how changes in the $\sigma-\varepsilon$ curves might affect autohesive tack (6, 8, 36, 45). An increase in the modulus, or σ_{max}, could cause a reduction in the contact area and result in a reduction in bond strength. An increase in W_b represents the potential for dissipating a greater amount of energy during bond separation and, therefore, increasing the bond strength. However, in order to realize this potential, W_b must be increased without increasing the modulus, so that bond formation is not impeded. In order for this to occur, ε_b must increase (45). Figure 5a shows that the addition of nanoclay increases Young's modulus of EPDM rubber. The increase in the elastic modulus (determined at low strain) of EPDM rubber with the concentration of nanoclay elucidates the reinforcing action of nanoclay. In addition, incorporation of nanoclay increases the area under the $\sigma-\varepsilon$ curve by concomitantly increasing the maximum tensile stress and the percentage of elongation. It seems that up to a concentration of 4 phr of nanoclay, the increase in σ_{max} is not high enough to totally retard the bond formation ability, and the W_b value is sufficiently large to dissipate a greater amount of energy during the bond separation process. Hence, the tack strength increases. However, at a concentration of 8 phr of nanoclay, the increase in σ_{max} must be high enough to retard the bond formation ability, and hence the tack strength starts to decrease. Therefore, the incorporation of nanocaly into EPDM rubber at a 4 phr concentration appears to have the ideal effect.

From the existing literature, it is well known that in order to achieve a high tack or peel strength, a polymer must be sufficiently viscoelastic (liquid-like) to enable fibrillation (46, 47). Very recently, Deplace et al. (46) and Creton et al. (47) have shown a good analogy between the plateau stress of the probe tack test and the tensile test. Roberts (45) has proposed that during the bond separation process in the peel test of the autohesive tack joints, the strength of the local bonds will be sufficient to cause fibrils to be drawn from the surfaces. Finally, the fibrillar structure will detach from the surface. Glassmaker et al. (48) have suggested that the detachment of the fibrils from the surface of the probe (in probe tack test) is controlled by the strain hardening of the polymer in the fibrils. Here, the addition of nanoclay reasonably increases the elastic modulus of the EPDM rubber (see Figure 5a), and therefore the strength of the rubber in the fibril of the filled samples is higher when compared to their unfilled counterpart.

Kumar et al. (10) have shown that among the different tackification mechanisms, the polar groups in the tackifiers under some stringent conditions can significantly contribute to an increase in the tack strength by increasing the surface energy of the base elastomer. However, here, the addition of nanoclay does not alter the surface energy of EPDM rubber. The surface energy values of samples EP and EPNA4 are 33.0 mJ/m^2 and 34.5 mJ/m^{2,} respectively. Therefore, the surface region of the clay loaded samples also remains rubbery, and hence there will be adequate wetting at the interface for the bond formation. Very recently, Kumar et al. (35, 36) reported that the addition of sepiolite and MMT nanoclay to BIMS rubber does not alter the surface properties of the rubber.

3.3. Dynamic Mechanical Analysis (DMA). ***3.3.1. Temperature Sweep Studies.*** Dynamic mechanical analysis (DMA) can provide deep insight into the tack performance of the rubber−clay mixtures (36, 49, 50). The plots of tan σ (the ratio of E''/E' or the damping factor), loss modulus (E''), and storage modulus (E') against temperatures for representative samples are shown in Figure 6a,b. Generally, for most of the polymers, the tan δ peak occurs at the glass transition temperature (T_g) of the polymer. However, it has also been reported that the tan δ peak cannot be identified with the glass transition temperature (T_g) because its position shifts depending on the value of the rubbery modulus, which changes due to the presence of fillers (51). Therefore, it has been pointed out that the peak of the loss modulus should be used to identify T_g (51).

Here, the T_g value of the neat EPDM rubber and the nanocomposites (from the tan δ peak) is located at −43 °C (Figure 6a), whereas the same from the loss modulus peak occurs at −49 °C (Figure 6a). Robertson et al. have reported that the T_g determined from tan δ is always 7−10 °C higher as compared to the same evaluated from the loss modulus curve (51). Interestingly, a similar type of observation has been observed here also. The tan δ peak temperature and loss modulus peak temperature of neat EPDM rubber have not been altered by the addition of nanoclay (Table 2). The height of the tan δ peak also remains unchanged with an increasing clay content up to 8 phr (Table 2). In the case of pressure sensitive adhesion measured by the probe tack test,

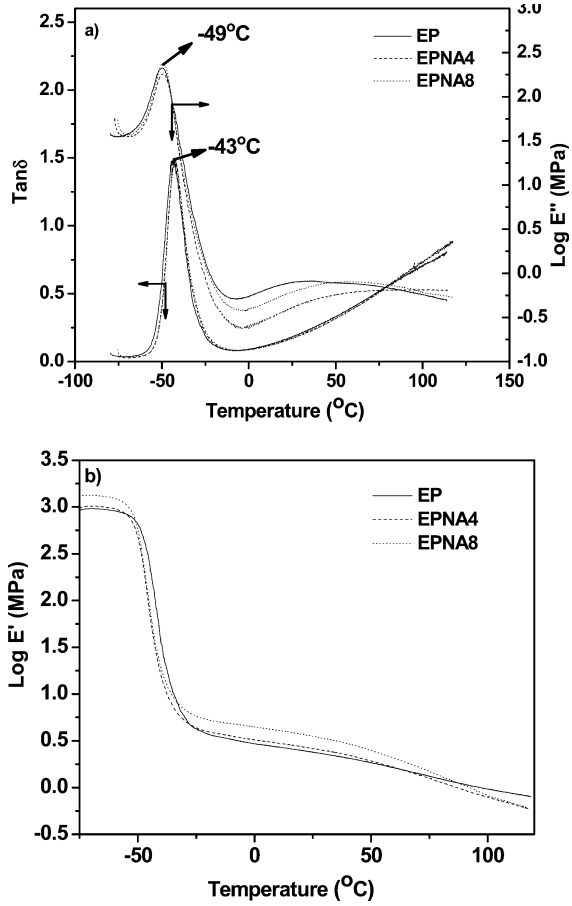

FIGURE 6. (a) Tan δ and log E'' vs temperature curves of EP, EPNA4, and EPNA8. (b) Log E' vs temperature curves of EP, EPNA4, and EPNA8.

it is generally expected that the tan δ value needs to increase in order to get fibrillation, and the fibrils can extend more without detaching themselves from the substrate to provide a higher tack strength (49). The tan δ value of the sample EP at room temperature of ca. 25 °C (the temperature at which peel tests were performed) also remains unaltered by the addition of nanoclay. For instance, the tan δ values of the samples EP and EPNA4 at 25 °C are the same (0.18). Therefore, during peeling of the clay loaded samples at 25 °C, the extent of fibrillation will not be hampered due the presence of nanoclay. But, the strength of the rubber in the fibril of the clay loaded samples is higher when compared to their unfilled counterpart due to the nanoclay reinforcement. Consequently, the tack strength of the clay loaded samples is higher.

On the other hand, the plateau modulus, E_n^0, values of the unfilled EPDM rubber increase with the increase in loading of nanoclay (Figure 6b). The DMA results are in line with the mechanical properties. The increase in storage modulus values by the addition of nanoclay clearly elucidates the interaction between the nanoclay and the EPDM rubber.

It is well known that the self-diffusion of rubber molecules at the tack junction is highly governed by the entanglement density in the rubbery plateau zone, which can be accurately determined from the entanglement molecular weight (M_e). This can be estimated from the plateau modulus as follows (52−55):

$$M_e = \frac{\rho RT}{E_n^0} \quad (4)$$

where ρ is the density of the polymer or blend, R is 8.31 × 10^7 J/(mol K), T is the absolute temperature where E_n^0 is located, and E_n^0 is determined from the storage modulus (E') at the onset of the rubbery region (usually where tan δ reaches a minimum following the prominent maximum). The E_n^0 and M_e values of the neat EPDM rubber and the nanocomposites are reported in Table 2. It is observed that the M_e value slightly decreases with the addition of 4 phr nanoclay. On the other hand, there is an abrupt decrease in the M_e value with the incorporation of 8 phr of nanoclay. Therefore, considering these results coupled with the earlier results, it can be inferred that at a concentration of 4 phr of nanoclay, the increase in the entanglement density is not high enough to eliminate the diffusion of elastomer chains across the interface, and the diffused chains should show greater resistance to separation due to the higher cohesive strength of the matrix. Hence, the tack strength is very high. However, at a concentration of 8 phr of nanoclay, the increase in the entanglement density must be sufficiently high to eliminate the diffusion of elastomer chains across the interface, which will reduce the tack strength.

3.3.2. Frequency Sweep Studies. From the frequency sweeps at different temperatures, master curves were constructed by using the time−temperature superposition principle. Figure 7 shows the log E' vs log reduced frequency master curves of EP, EPNA4, and EPNA8 at a reference temperature of 25 °C. Here, it should be pointed out that the master curves that extend through the glass transition zone may not be quantitative because the shift factors are different for the chain modes and the segmental modes, both of which contribute in the transition zone (56). As the glass transition temperature is constant, Figures 8 and 9 have been drawn showing the logarithmic plots of log E' and log E'' master curves against the log reduced frequency for EP and EPNA4 at 25 °C. The plots of other samples are not shown here. These figures clearly illustrate the different zones (terminal, plateau, transition, and glassy zones) of viscoelastic behavior of neat EPDM rubber (EP) and 4 phr

Table 2. Effect of Nanoclay on the Viscoelastic Properties of the EPDM Rubber

sample number	designation	T_g from tan δ peak temperature (°C)	T_g from loss modulus peak temperature (°C)	tan δ peak height	plateau modulus, E_n^0 (MPa)	entanglement molecular weight, M_e (g/mol)
1	EP	−43	−49	1.48	3.07	726
2	EPNA4	−43	−49	1.48	3.35	666
3	EPNA8	−43	−49	1.48	4.56	491

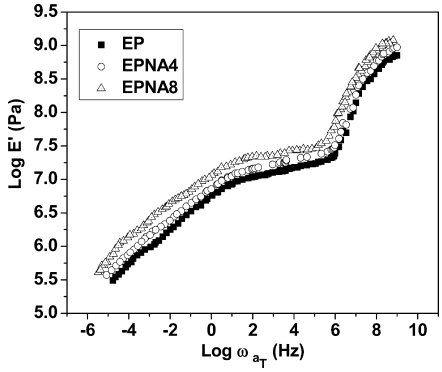

FIGURE 7. Master curves of log E' vs the log reduced frequency at 25 °C for EP, EPNA4, and EPNA8.

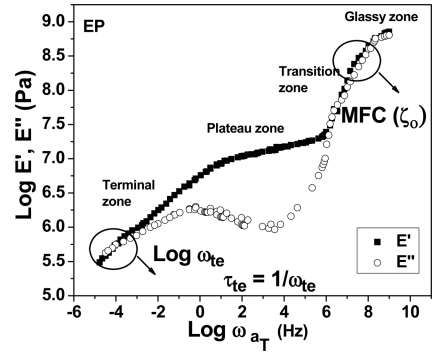

FIGURE 8. Master curve of log E' and log E'' vs the log reduced frequency at 25 °C for EP.

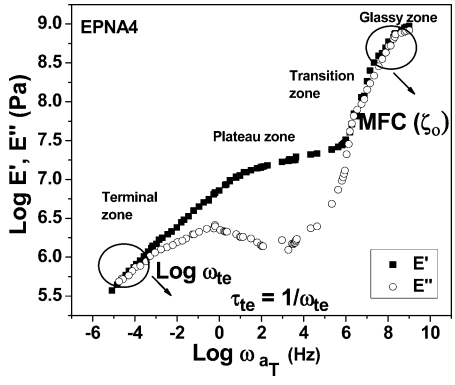

FIGURE 9. Master curve of log E' and log E'' vs the log reduced frequency at 25 °C for EPNA4.

of the clay loaded sample (EPNA4). Several molecular parameters of the polymers, and in particular their terminal relaxation time (τ_{te}) and the monomer friction coefficient (ζ_0), can be extracted from the crossover frequency (ω_c), where E' and E'' intersect (as shown in Figures 8 and 9) (57, 58). Similar to EP, EPNA4 and EPNA8 also obey the time−temperature superposition principle and display a linear viscoelastic region.

3.3.2.1. Terminal Relaxation Time (τ_{te}), Self-Diffusion Coefficient (D), and Monomer Friction Coefficient (MFC; ζ_0). de Gennes (59) has proposed the reptation model for the dynamics of entangled molecules in a network of fixed obstacles. According to this model, the polymer molecule slides or "reptates" through a "tube" whose contour is defined by the locus of entanglements with the neighboring molecules. Three characteristic times evolve from the description based on the dynamics of a molecule (60). Other workers advanced the knowledge further (57, 58, 60−63). Once the reptation time is identified, it is easy to calculate the self-diffusion coefficient (D). Accordingly, at 25°C, the self-diffusion coefficient (D) values of neat EPDM rubber and EPDM−nanoclay mixtures can be calculated from the equation given below (64)

$$D = \frac{(R_g)^2}{2\tau_{rep}} \tag{5}$$

where R_g is the radius of gyration of EPDM rubber and τ_{rep} is the reptation time. For EPDM rubber, the R_g value has been calculated as 9.69 nm from eq 3.

The monomer friction coefficient is the average resistance force per monomer unit encountered when a polymer chain moves through its surroundings at a unit speed (65, 66). By assuming that the Rouse model describes the high frequency response of the long chains in the transition zone, we have (65, 66):

$$E'(\omega) = E''(\omega) = \rho\nu_0 N_a R_g \sqrt{\frac{\zeta_0 kT\omega}{8m_0 M}} \tag{6}$$

where $E'(\omega)$ and $E''(\omega)$ are the storage and loss modulii, ω is the frequency, ρ is the density, N_a is Avogadro's number, ν_0 is the volume fraction of the base polymer, R_g is the radius of gyration, k is the Boltzmann constant, T is the absolute temperature, m_0 is the monomer molecular weight, and M is the molecular weight of the base polymer.

At this juncture, it is noteworthy to compare and understand the actions of nanoclay and tackifiers in low frequency and high frequency zones of the DMA frequency sweep master curves. Generally, in a low frequency zone, the addition of a compatible tackifier results in a reduction of the storage modulus; simultaneously, the storage modulus increases at higher rates (high frequency zone) relative to that of the neat rubber (10, 67−69). It has been suggested by previous researchers that this favors high tack because the behavior at the low frequency zone in the frequency sweep master curves can be related to the bonding formation process of the tack test because the bond formation is a very low rate process (3, 67−69). On the other hand, the behavior high frequency zone in the frequency sweep master curves can be related to the debonding process of the tack test because the bond strength is measured at higher rates (67−69).

However, here, the addition of nanoclay increases the storage modulus over the entire frequency scale range (see Figure 7), which is contrary to the action of the tackifier. However, the tack strength prominently increases by the addition of nanoclay up to a certain concentration. The possible reason for this behavior has been explained below with the help of various viscoelastic parameters such as terminal relaxation time (τ_{te}), the self-diffusion (D) coefficient, and the monomer friction coefficient (ζ_0) extracted

Table 3. Relaxation Time (τ), Self-Diffusion (D), and Monomer Friction Coefficient (ζ_0) Values of EP, EPNA4, and EPNA8

sample number	designation	log ζ_0 (g/s)	τ_{te} (s)	D (m^2/s)
1	EP	0.003	31622	1.48×10^{-21}
2	EPNA4	0.007	35481	1.32×10^{-21}
3	EPNA8	0.012	44668	1.05×10^{-21}

from DMA frequency sweep master curves, and their values are listed in Table 3.

From Table 3, it is seen that the terminal relaxation time (τ_{te}) of the neat EPDM rubber increases with the concentration of nanoclay. This suggests that the nanoclay imposes more restrictions for the rubber molecules to disentangle, and hence the terminal relaxation times (τ_{te}) of clay loaded samples are higher when compared to their unfilled counterparts. It can also be seen that the addition of 4 phr of nanoclay (EPNA4) to EPDM marginally increases the terminal relaxation time. On the other hand, there is a considerable difference between the terminal relaxation time values of EP and EPNA8. This is also reflected in the differences of the entanglement molecular weight values (compare M_e values in Table 2 for EP and EPNA8). This effect can be attributed to the relatively higher concentration of nanoclay in the EPDM matrix, which can increase the terminal relaxation time either through excessive reinforcement or the aggregated nanoclay particles can themselves act as topological constraints for the elastomer chains to disentangle and reptate. The self-diffusion coefficient (D) values calculated from eq 5 for samples EP, EPNA4, and EPNA8 are reported in Table 3. From Table 3, it is seen that the self-diffusion coefficient value of EPDM rubber decreases with the nanoclay concentration, which is ascribed to the restriction in molecular mobility [longer terminal relaxation time (τ_{te})] in the presence of nanoclay.

In the transition zone, the monomer friction coefficient values of EP, EPNA4, and EPNA8 have been calculated from eq 6, and the values are listed in Table 3. The monomer friction coefficient value increases with the addition of the nanoclay. The possible reason for the increment of the monomer friction coefficient value by the addition of nanoclay can be due to the reinforcing action of the nanoclay in the EPDM matrix, which will restrict the segmental mobility. This seems to indicate that when the clay concentration is 4 phr, the diffusion of elastomer chains across the interface is sufficient to establish entanglements, and the entangled chains show greater resistance to separation due to the higher monomer friction coefficient value. Hence, the tack strength is enhanced.

3.4. Effect of Nanoclay on the Microstructure of EPDM rubber through WAXD. The X-ray diffraction spectrum of neat EPDM rubber (unstrained condition) shows a peak at approximately 19°, which corresponds to the amorphous PE (Figure 10) (70). EPNA4 also portrays a peak at 19° in the unstrained state (Figure 10). However, it is interesting to note that there is some reduction in the height of this peak by the addition of nanoclay, which can be attributed to the disruption of the crystallites in the EPDM

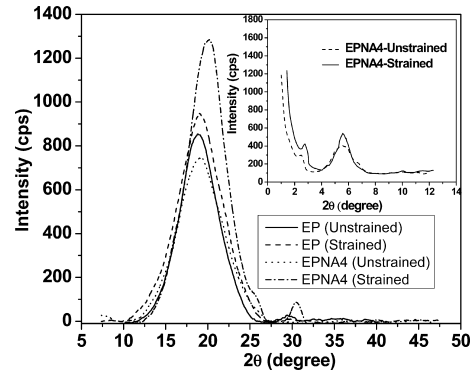

FIGURE 10. XRD patterns of EP and EPNA4 under unstrained and strained conditions (in higher angle range). (Inset) XRD patterns of EPNA4 under unstrained and strained conditions in the low angle region.

rubber by the addition of nanoclay. This suggests that the incorporation of nanoclay into EPDM rubber can reduce the amount of crystallites that are already present in the unstressed state, and therefore the chain mobility required for tack bond formation can be achieved.

It is also very much necessary to have an idea about the effect of straining (i.e., here while peeling the samples) on the SIC phenomena of EPDM rubber in the presence and absence of nanoclay. Therefore, the samples were strained to about 150% elongation at room temperature for about 15 s, and then the XRD studies were performed at room temperature. The strain was released prior to the XRD experiment. After straining the neat EPDM rubber, the height of the peak obtained at 19° slightly increases (see Figure 10). This diffraction pattern obtained in this way indicates that a part of the terpolymers crystallizes while straining. This observation is in line with the results reported by earlier researchers (71−74). Bassi et al. (70) have found an elegant relationship between the degree of straining and degree of crystallinity in an unfilled EPDM terpolymer. On the other hand, after straining the clay loaded sample (EPNA4), the peak shifts towards a higher 2θ value (20.1°) and becomes sharper, and the height of the peak drastically increases when compared to its stretched unfilled counterpart (see Figure 10). Although the 2θ value (20.1°) is lower than the 2θ value of the crystalline peak in PE (21.5°), this peak should also correspond to the crystalline peak of PE segments, since it has been well established that the position of the crystalline peak of PE will shift to low angles on the basis of the propylene content in EPDM (75). Another new peak also arises at 29° (as shown in Figure 10) after straining the clay loaded sample. These clearly exemplify that the presence of nanoclay can significantly increase the SIC of EPDM rubber during straining. Furthermore, from the inset of Figure 10, it can be seen that compared to the XRD curve before straining (EPNA4 in unstrained condition), the intensity of the characteristic peaks of clay layers at 5.46 nm enhances after straining, indicating that the clay layers arrange more during straining. This result is consistent with a high degree of orientation of silicate layers under uniaxial strain in butadiene rubber or SBR-containing organic layered silicates, which was monitored by means of online WAXS

measurements (76). In the case of NR−nanoclay mixtures also, it has been reported that the presence of nanoclay will increase the SIC due to the alignment of nanoclay particles during straining (77). The same explanations can be applicable here for EPDM−nanoclay mixtures also. Due to the significant increase in percentage crystallinity during straining, the clay loaded samples will act as additional physical crosslinks to enable more macromolecules to orient, and thus, the highly oriented microfibrillar structure and more oriented amorphous chains during peeling should provide greater bond separation resistance to the diffused chains. Here, it should be pointed out that the addition of nanoclay favors a higher tack strength for EPDM rubber through its synergetic effect. The nanoclay reduces the percentage crystallinity in the unstressed state and facilitates the diffusion of elastomer chains across the interface; simultaneously, it increases the percentage crystallinity during straining and imparts greater bond breaking resistance. This is a very unique and interesting observation that has been reported for the first time ever in the literature.

4. CONCLUSIONS

The influence of unmodified MMT nanoclay on the autohesive tack strength of EPDM rubber has been investigated using a 180° peel test. The following conclusions are drawn from this study. The X-ray diffraction (XRD), atomic force microscopy (AFM), and transmission electron microscopy (TEM) studies show an intercalated morphology of nanoclay in the EPDM matrix up to a concentration of 4 phr of clay, beyond which an agglomerated morphology has been observed. The nanoclay particles exert a significant increase in the tack strength of EPDM rubber. For example, the tack strength of 4 phr of nanoclay loaded EPDM rubber is approximately 137% higher than the tack strength of unfilled EPDM rubber. However, at higher concentrations of nanoclay (> 4 phr), the tack strength starts to decrease. There is an increase in green strength of EPDM rubber with the concentration of nanoclay. In the tensile stress−strain curves, the incorporation of nanoclay increases the elastic modulus of the EPDM rubber, and hence the strength of the rubber in the fibrils formed during the separation process of the clay loaded samples is higher when compared to their unfilled counterpart. This phenomenon significantly contributes to the enhancement of the tack strength.

From the dynamic mechanical analysis (DMA), temperature sweep, and frequency sweep studies, it has been observed that the addition of nanoclay reduces the extent of self-diffusion (D) of EPDM rubber molecules at the tack junction (by increasing the terminal relaxation time, τ_{te}) due to the reinforcing action of the nanoclay. When the clay concentration is 4 phr, the extent of diffusion across the interface is still sufficient to establish entanglements on either side of the interface, and the entangled chains offer more resistance to separation upon stressing due to the existence of a higher monomer friction coefficient (ζ_0) in the nanocomposite when compared to the unfilled sample. On the other hand, when the clay concentration is higher (> 4 phr), the extent of diffusing elastomer chains across the interface is drastically reduced so that the physical links could not be established across the interface by interdiffusion, which results in a lower tack strength. The mixing of nanoclay with EPDM rubber reduces the percentage of crystallinity of EPDM rubber in the unstrained state, and therefore the chain mobility required for interdiffusion is increased. Moreover, the presence of nanoclay in the EPDM matrix enhances the overall crystallization tendencies of the EPDM chains while straining due to the alignment of nanoclay particles, which helps to increase the stress (work) required to debond. In addition, rearrangement of the crystals in the rubber matrix could also provide an additional energy dissipation mechanism.

Acknowledgment. G.C.B. would like to thank All India Council for Technical Education (AICTE), New Delhi for financial support.

REFERENCES AND NOTES

(1) Kramer, E. J. *Mat. Res. Soc. Symp. Proc.* **1985**, *40*, 227–237.
(2) Voyutskii, S. S. *Autohesion & Adhesion of High Polymers*; Interscience Publishers: New York, 1963; Chapters 1 and 2, pp 5−59.
(3) Hamed, G. R. *Rubber Chem. Technol.* **1981**, *54*, 576–595.
(4) Aradian, A.; Raphael, E.; de Gennes, P.-G. *Macromolecules* **2000**, *33*, 9444–9451.
(5) Kim, Y. H.; Wool, R. P. *Macromolecules* **1983**, *16*, 1115–1120.
(6) Hamed, G. R.; Roberts, G. D. *J. Adhes.* **1994**, *47*, 95–113.
(7) Bhowmick, A. K.; De, P. P.; Bhattacharyya, A. K. *Polym. Eng. Sci.* **1987**, *27*, 1195–1202.
(8) Kumar, K. D.; Tsou, A. H.; Bhowmick, A. K. *J. Adhes. Sci. Technol.* **2008**, *22*, 2039–2058.
(9) Basak, G. C.; Bandyopadhyay, A.; Bhowmick, A. K. *Int. J. Adhes. Adhes.* **2010**, *30*, 489–499.
(10) Kumar, K. D.; Tsou, A. H.; Bhowmick, A. K. *J. Polym. Sci., Part B: Polym. Phys.* **2010**, *48*, 972–982.
(11) Beatty, J. R. *Rubber Chem. Technol.* **1969**, *42*, 1040–1053.
(12) Busse, W. F.; Lambert, J. M.; Verdery, R. B. *J. Appl. Phys.* **1946**, *17*, 376–385.
(13) Beckwith, R. K.; Welch, L. M.; Nelson, J. F.; Chaney, A. L.; McCracken, E. A. *Rubber Chem. Technol.* **1950**, *23*, 933–944.
(14) Kumar, B.; De, P. P.; De, S. K.; Peiffer, D. G.; Bhowmick, A. K. *J. Adhes. Sci. Technol.* **2001**, *15*, 1145–1163.
(15) Bhaumik, T. K.; Gupta, B. R.; Bhowmick, A. K. *J. Adhes. Sci Technol.* **1987**, *1*, 227–238.
(16) van Gunst, C. A.; Paulen, H. J. G.; Wolters, E. *Kautsch. Gummi Kunstst.* **1975**, *12*, 714–720.
(17) Ruch, F.; David, M.-O.; Vallat, M.-F.; Schultz, J. *C. R. Acad. Sci., Ser. IIB: Mech. Phys. Astron.* **1999**, *327*, 1089–1094.
(18) Vaia, R. A.; Lincoln, D. In *Polymer Nanocomposites: Synthesis, Characterization and Modeling*; Krishnamoorti, R., Vaia, R. A., Eds.; ACS Symposium Series No. 804, American Chemical Society: Washington, DC, 2000; Chapter 9, p 102.
(19) Ray, S. S.; Okamoto, M. *Prog. Polym. Sci.* **2003**, *28*, 1539–1641.
(20) Maiti, M.; Bhattacharya, M.; Bhowmick, A. K. *Rubber Chem. Technol.* **2008**, *81*, 384–469.
(21) Sadhu, S.; Bhowmick, A. K. *J. Polym. Sci., Part B: Polym. Phys.* **2004**, *42*, 1573–1585.
(22) Maiti, M.; Bhowmick, A. K. *J. Polym. Sci., Part B: Polym. Phys.* **2006**, *44*, 162–176.
(23) Maiti, M.; Bhowmick, A. K. *Comp. Sci. Tech.* **2008**, *68*, 1–9.
(24) Bhattacharya, M.; Bhowmick, A. K. *Polymer* **2008**, *49*, 4808–4818.
(25) Bhattacharya, M.; Maiti, M.; Bhowmick, A. K. *Polym. Eng. Sci.* **2009**, *49*, 81–98.
(26) Choudhury, A.; Bhowmick, A. K.; Ong, C. *Polymer* **2009**, *50*, 201–210.
(27) Maji, P. K.; Guchhait, P. K.; Bhowmick, A. K. *ACS Appl. Mater. Interfaces* **2009**, *1*, 289–300.
(28) George, J. J.; Bhowmick, A. K. *Nanoscale Res. Lett.* **2009**, *4*, 655–664.

(29) Sahoo, S.; Bhowmick, A. K. *J. Appl. Polym. Sci.* **2007**, *106*, 3077–3083.
(30) Sahoo, S.; Bhowmick, A. K. *Rubber Chem. Technol.* **2007**, *80*, 826–837.
(31) Ganguly, A.; Bhowmick, A. K.; Li, Y. *Macromolecules* **2008**, *41*, 6246–6253.
(32) Sengupta, R.; Bandyopadhyay, A.; Sabharwal, S.; Chaki, T. K.; Bhowmick, A. K. *Polymer* **2005**, *46*, 3343–3354.
(33) Datta, H.; Bhowmick, A. K.; Singha, N. K. *Polymer* **2009**, *50*, 3259–3268.
(34) Patel, S.; Bandyopadhyay, A.; Ganguly, A.; Bhowmick, A. K. *J. Adhes. Sci. Technol.* **2006**, *20*, 371–385.
(35) Kumar, K. D.; Tsou, A. H.; Bhowmick, A. K. *J. Adhes. Sci. Technol.* **2010**, *24*, 789–809.
(36) Kumar, K. D.; Tsou, A. H.; Bhowmick, A. K. *Macromolecules* **2010**, *43*, 4184–4193.
(37) Spelt, J. K.; Neumann, A. W. *Langmuir* **1987**, *3*, 588–591.
(38) Sen Majumder, P.; Bhowmick, A. K. *Radiat. Phys. Chem.* **1998**, *53*, 63–78.
(39) Basak, G. C.; Bandyopadhyay, A.; Bharadwaj, Y. K.; Sabharwal, S.; Bhowmick, A. K. *J. Adhes. Sci. Technol.* **2009**, *23*, 1763–1786.
(40) Chang, R.-J.; Gent, A. N. *J. Polym. Sci., Part B: Polym. Phys.* **1981**, *19*, 1619–1633.
(41) Zosel, A. *Colloid Polym. Sci.* **1985**, *263*, 541–553.
(42) Chanda, M. *Introduction to Polymer Science and Chemistry: A Problem Solving Approach*; CRC Press, Taylor and Francis group: Boca Raton, FL, 2006; Chapter 3, pp 160—165.
(43) Usuki, A.; Tukigase, A.; Kato, M. *Polymer* **2002**, *43*, 2185–2189.
(44) Bhattacharya, M.; Maiti, M.; Bhowmick, A. K. *Rubber Chem. Technol.* **2008**, *81*, 782–808.
(45) Roberts, G. D. Ph.D. Thesis, University of Akron: Akron, OH, 1991.
(46) Deplace, F.; Carelli, C.; Mariot, S.; Retsos, H.; Chateauminois, A.; Okzineb, K.; Creton, C. *J. Adhes.* **2009**, *85*, 18–54.
(47) Creton, C.; Hu, G.; Deplace, F.; Morgret, L.; Shull, K. R. *Macromolecules.* **2009**, *42*, 7605–7615.
(48) Glassmaker, N. J.; Hui, C. Y.; Yamaguchi, T.; Creton, C. *Eur. Phys. J. E.* **2008**, *25*, 253–266.
(49) Wang, T.; Colver, P. J.; Bon, S. A. F.; Keddie, J. L. *Soft. Matter.* **2009**, *5*, 3842–3849.
(50) Wang, T.; Lei, C.-H.; Dalton, A. B.; Creton, C.; Lin, Y.; Fernando, K. A. S.; Sun, Y.-P.; Manea, M.; Asua, J. M.; Keddie, J. L. *Adv. Mater.* **2006**, 2730–2734.
(51) Robertson, C. G.; Lin, C. J.; Rackaitis, M.; Roland, C. M. *Macromolecules* **2008**, *41*, 2727–2731.
(52) Ferry, J. D. *Viscoelastic Properties of Polymers*, 3rd ed.; Wiley: New York, 1982; Chapter 13, pp 366—403.
(53) Cooper-White, J. J.; Mackay, M. E. *J. Polym. Sci., Part B: Polym. Phys.* **1999**, *37*, 1803–1814.
(54) Tobing, S. D.; Klein, A. *J. Appl. Polym. Sci.* **2000**, *76*, 1965–1976.
(55) Yuan, B.; McGlinchey, C.; Pearce, E. M. *J. Appl. Polym. Sci.* **2006**, *99*, 2408–2413.
(56) Plazek, D. J. *J. Rheol.* **1996**, *40*, 987–1014.
(57) Schach, R.; Creton, C. *J. Rheol.* **2008**, *52*, 749–767.
(58) Schach, R.; Tran, Y.; Menelle, A.; Creton, C. *Macromolecules* **2007**, *40*, 6325–6332.
(59) de Gennes, P.-G. *Scaling Concepts in Polymer Physics*; Cornell University Press: Ithaca, NY, 1979.
(60) Karim, A.; Felcher, G. P.; Russell, T. P. *Macromolecules* **1994**, *27*, 6973–6979.
(61) Ferry, J. D.; Kramer, O. In *Science and Technology of Rubber*; Eirich, F. R., Ed.; Academic Press: New York, 1978; Chapter 5, pp 179—221.
(62) Prager, S.; Tirrell, M. *J. Chem. Phys.* **1981**, *75*, 5194–5198.
(63) Jud, K.; Kausch, H. H.; Williams, J. G. *J. Mat. Sci.* **1981**, *16*, 204–210.
(64) Roland, C. M.; Boehm, G. *Macromolecules* **1985**, *18*, 1310–1314.
(65) Colby, R. H.; Fetters, L. J.; Graessley, W. W. *Macromolecules* **1987**, *20*, 2226–2237.
(66) Tse, M. F. *J. Adhes. Sci. Tech.* **1989**, *3*, 551–570.
(67) Sheriff, M.; Knibbs, R. W.; Langley, P. G. *J. Appl. Polym. Sci.* **1973**, *17*, 3423–3438.
(68) Aubrey, D. W.; Sherriff, M. *J. Polym. Sci., Part A: Polym Chem* **1979**, *16*, 2631–2643.
(69) Kumar, K. D.; Gupta, S.; Tsou., A. H.; Bhowmick, A. K. *J. Appl. Polym. Sci.* **2008**, *110*, 1485–1497.
(70) Bassi, I. W.; Corradini, P.; Fegherazzi, G.; Valvassori, A. *Eur. Polym. J.* **1970**, *6*, 709–718.
(71) Walter, E. R.; Reding, E. P. *J. Polym. Sci.* **1956**, *21*, 561–562.
(72) Eichorn, R. M. *J. Polym. Sci.* **1958**, *31*, 197–198.
(73) Swann, P. R. *J. Polym. Sci.* **1962**, *56*, 409–416.
(74) Cole, E. A.; Holmes, D. R. *J. Polym. Sci.* **1960**, *46*, 245–256.
(75) Ma, Y.; Wu, Y. P.; Wang, Y. Q.; Zhang, L. Q. *J. Appl. Polym. Sci.* **2006**, *99*, 914–919.
(76) Ganter, M.; Gronski, W.; Reichert, P.; Mulhaupt, R. *Rubber Chem. Technol.* **2001**, *74*, 221–227.
(77) Carretero-Gonzalez, J.; Retsos, H.; Verdejo, R.; Toki, S.; Hsiao, B. S.; Giannnelis, E. P.; Lopez-Manchado, M. A. *Macromolecules* **2008**, *41*, 6763–6772.

AM100865N